CHEMISTRY
A EUROPEAN JOURNAL

DOI: 10.1002/chem.200601686

Electronic Properties of 3,3′-Dimethyl-5,5′-bis(1,2,4-triazine): Towards Design of Supramolecular Arrangements of N-Heterocyclic Cu^{I} Complexes

Blandine Courcot,[a] Diem Ngan Tran,[b] Bernard Fraisse,[a] François Bonhomme,[c] Alain Marsura,*[b] and Nour Eddine Ghermani[a, c]

In memory of Professor Guy Ourisson

Abstract: A new efficient and safe synthesis of 3,3′-dimethyl-5,5′-bis-(1,2,4-triazine) is presented. The electron-density distribution and electrostatic properties (charge, electrostatic potential) of this molecule were analyzed. These properties were derived from a high-resolution single-crystal X-ray diffraction experiment at 100 K and compared to the results obtained from ab initio DFT quantum-mechanical calculations. Comparisons of its electrostatic potential features and integrated atomic charges (quantum theory of atoms in molecules, QTAIM) have been made with those of related molecules such as bipyrimidine ligands. Two methods were used to derive integrated charges: one is based on the conventional analytical procedure and the second uses a steepest-ascent numerical algorithm. Excellent agreement was obtained between these two methods. Charges and electrostatic potential were used as predictive indices of metal chelation and discussed in the light of complexation abilities of the title compound and related molecules. The crystal structure of a Cu^{I} complex of 3,3′-dimethyl-5,5′-bis(1,2,4-triazine) is reported here. In the solid state, this complex forms a three-dimensional multibranch network with open channels in which counterions and solvent molecules are located. This architecture involves both *cis* and *trans* isomers of the title compound.

Keywords: ab initio calculations · copper · N ligands · nitrogen heterocycles · supramolecular chemistry

Introduction

Metallosupramolecular chemistry involves the use of combinations of organic ligands and metals for the construction of both discrete and polymeric aggregates. Nitrogen heterocycles are extensively used as bridging ligands in coordination chemistry, and the search of new ligands for novel self-assembled metallosupramolecular architectures remains of great interest. Among the nitrogen heterocycles, 2,2′-bipyridine has been widely used as the classical bidendate chelating heterocyclic ligand, along with its tridendate analogue terpyridine.[1a–c] Besides the pyridine ring, many other heterocycles which differ in their electronic and structural properties are often readily available by synthesis. Surprisingly, only a few of them have attracted the attention of coordination chemists. Nevertheless, some of them, for example, pyrazine, pyrazole, imidazole, and triazole, have been used as units for metal coordination.[1d–g]

Thus, taking in account that varying the heterocycle can effect dramatic changes in the physicochemical properties of metal complexes, we have reported original assemblies with bidendate heterocyclic ligands such as 4,4′-bipyrimidine,[2a–b] 2,2′-bipyrazine,[3a–b] 2,2′-bithiazole,[4a–b] 4,4′-bithiazole,[5] and their bipyridine–bipyrazine, bipyridine–bipyrimidine, and bipyridine–bithiazole heterotopic bis-bidendate combinations.[6a–c] Changes in the electronic structure of the ligands proved to have a major effect on complex configuration. For

[a] Dr. B. Courcot, Dr. B. Fraisse, Prof. N. E. Ghermani
Ecole Centrale Paris
Laboratoire SPMS UMR CNRS 8580 1
Grande Voie des Vignes, 92295 Châtenay-Malabry (France)

[b] D. N. Tran, Prof. A. Marsura
GEVSM, UMR CNRS 7565
Structure et Réactivité des Systèmes Moléculaires Complexes
Université Henri Poincaré Nancy-1
5 rue A. Lebrun, BP 403, 54250 Nancy (France)
Fax: (+33) 383-682-345
E-mail: Alain.Marsura@pharma.uhp-nancy.fr

[c] Dr. F. Bonhomme, Prof. N. E. Ghermani
Laboratoire PPB, UMR CNRS 8612, IFR 141
Faculté de Pharmacie 5, rue Jean-Baptiste Clément
92296 Châtenay-Malabry (France)

example, with the ligand combinations, high selectivity for head-to-tail (H–T) or head-to-head (H–H) orientation of the ligand strands around the metal centers in the resultant crystal structures was observed with different metals.[6a–c] Such a selectivity has never been obtained before when induced, for example, only by steric hindrance. This was recently investigated by us at a theoretical level that established the π-backbonding effect, when effective, to be at the origin of the strongly orientational behavior.[7]

Continuing our research on new bis-heterocyclic systems, we decided to explore the metal-coordination capabilities of the 3,3′-dimethyl-5,5′-bis(1,2,4-triazine) ligand. We report here a new synthesis of this ligand and its X-ray structure and electron-density distribution from both experiment and theory. As far as we know only one study on the isomeric bis-3,3′-(5,6-dimethyl-1,2,4-triazine) Fe^{II} complexes has been reported,[8] whereas nothing has been published on the metal complexes of the 3,3′-dimethyl-5,5′-bis(1,2,4-triazine) isomer. In the present study, the crystal structure of the Cu^{I} complex of this ligand is reported and is compared to those of related molecules.

Results and Discussion

Synthesis: Substituted and unsubstituted 5,5′-bis(1,2,4-triazines) have been generally synthesized in one step from the unsubstituted or substituted 1,2,4-triazine heterocycles by a simple coupling reaction under strongly basic conditions or by treatment with potassium cyanide.[9a–c] The 1,2,4-triazine starting materials have been synthesized by intermolecular heterocyclization between amidrazones[10a–b] or thiosemicarbazides[11] and α,β-dicarbonyl compounds. Here we are interested in 3,3′-dimethyl-5,5′-bis(1,2,4-triazine), which was obtained by two methods from acetamidrazone (**1**; Scheme 1). The authors recommended using anhydrous hydrazine, a very hazardous reagent, for the synthesis of 3-methyl-1,2,4-triazine (**2**). To circumvent the dangerous and difficult preparation of anhydrous hydrazine for obtaining acetamidrazone, we advantageously used the stable and harmless hydrazine/hydroquinone (1/1) inclusion complex,[12] which afforded **1** in good yield (60%). Bis-triazine **3** could be synthesized efficiently in only one step from **1** without isolation of 3-methyl-1,2,4-triazine (**2**) and in fairly good yield (55%). Moreover, acetamidrazone (**1**) could be obtained quantitatively from acetamidine hydrochloride by using commercial hydrazine hydrate ($N_2H_4{\cdot}H_2O$) solution, which contains 32% of water and is totally safe.

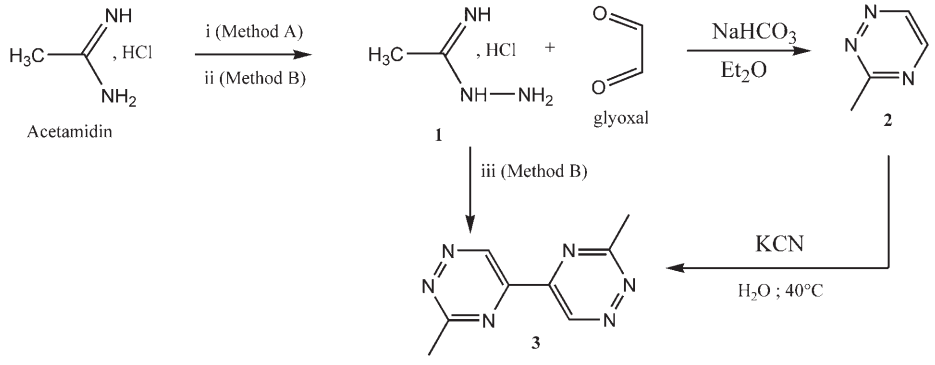

Scheme 1. Synthesis of **3**. i) NH_2NH_2/hydroquinone complex/MeOH; 0–5 °C; ii) NH_2NH_2, H_2O; $MgSO_4$; iii) KOH; K_2CO_3/KCN; 40 °C.

Molecular conformation and crystal stacking of 3: An ORTEP[13] plot of 3,3′-dimethyl-5,5′-bis(1,2,4-triazine) (**3**) is given in Figure 1. The molecule is in the *s-trans* conformation in the solid state and is not rigorously planar. The dihedral angle C6′-C5′-C5-C6 is 173.63(6)°. The C5–C5′ bond length of 1.4813(7) Å is slightly shorter than that in 2,2′-dimethyl-6,6′-diphenyl-4,4′-bipyrimidine (**4**; C4–C4′ 1.4891(7) Å) at 100 K.[2] The N heterocycle in **3** exhibits alternately short and long bond lengths: C5–N4 1.3250(7), N4–C3 1.3468(7), C3–N2 1.3380(8), N2–N1 1.3399(7), N1–C6 1.3280(8), and C6–C5 1.4056(8) Å. The values obtained for the second triazine ring are within the estimated standard deviations. No hydrogen bonding occurs in the crystal stacking, which displays parallel zigzag arrangements of molecules (Figure 2).

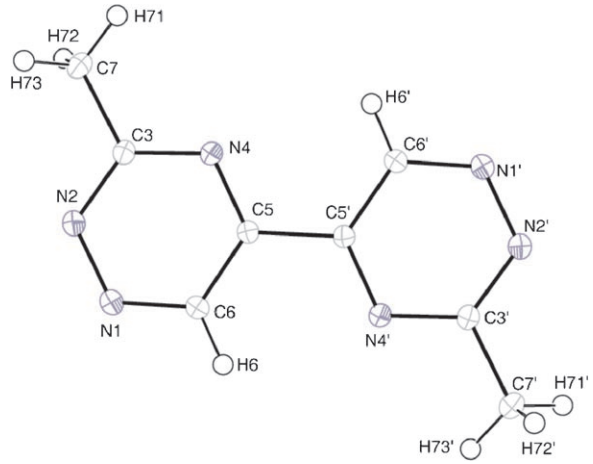

Figure 1. ORTEP[13] plot and atom-numbering scheme of **3**. Ellipsoids are at the 50% probability level.

Electron deformation density of 3: The presence of three nitrogen atoms in the triazine ring, two of which are bonded together, is expected to strongly perturb the electron distribution in this group. One way to visualize the anisotropy of the electron density is to plot the

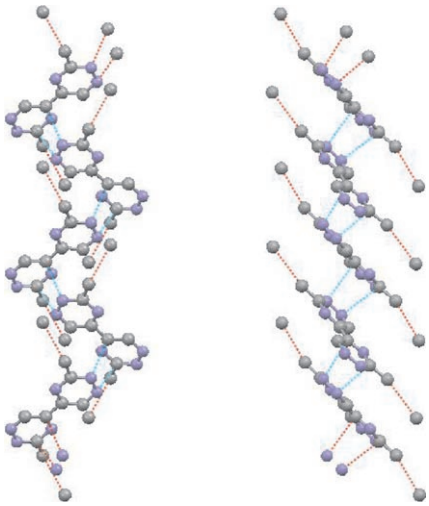

Figure 2. Two views of the crystal stacking of **3** along the *b* axis. Hydrogen atoms are omitted for clarity and nitrogen atoms are in blue. Dashed lines indicate short contacts between adjacent molecules.

electron deformation density, that is, the difference between the total electron density and that obtained as a superposition of isolated neutral-atom densities (promolecule). Figure 3 displays the theoretical and static experimental

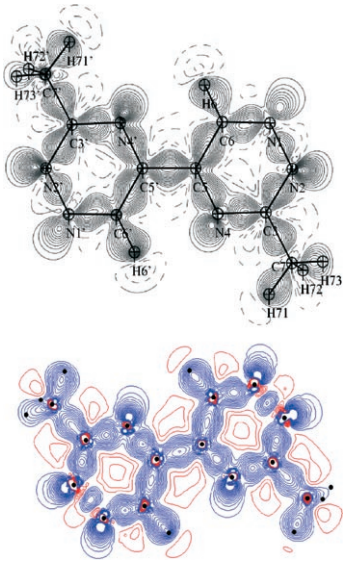

Figure 3. Static experimental electron deformation (top) and theoretical (bottom) densities of **3**. Contour intervals 0.05 e Å^{-3}; negative contours are dashed in experimental maps and are in red in theoretical map.

electron deformation densities in the plane defined by N4, C5, and C5′ of **3**. These maps exhibit similar features for the C–C, C–N, and C–H bonds, with an average accumulation of electron density of around 0.6 e Å^{-3}, as is generally found in organic molecules. A good agreement between theory and experiment is found for the electron-density peak in the N1–N2 bond of about 0.4 to 0.5 e Å^{-3}. This value compares quantitatively well with those obtained for N–N bonds in the tetrazole ring of LR-B/081 reported by Destro et al.[14] Accumulation of electrons in lone pairs on nitrogen atom are well resolved in these two maps. However, the contractions of these lone pair electrons are different for the three nitrogen atoms of the triazine ring in the experimental map (Figure 3, top), whereas in the theoretical electron-density map (Figure 3, bottom), the three nitrogen atoms exhibit an almost identical contraction of the lone pairs. Slight discrepancies also appear for hydrogen atoms, which display relatively higher polarizations in the experimental electron density map than in the theoretical one.

Electrostatic potential of 3 and related molecules: In an attempt to relate the electronic properties of N-heterocyclic compounds to their chelation of metals, we compared the electrostatic potential obtained from both experiment and theory. The molecular electrostatic potential of **3** is shown in Figure 4. As expected, the areas of negative electrostatic po-

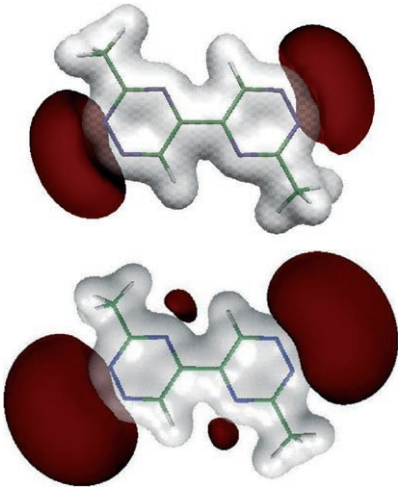

Figure 4. Electrostatic potential of **3**. Top: from experiment. Bottom: from theory. Gray and dark red isosurfaces correspond to +0.20 and −0.05 e Å^{-1}, respectively. The orientation of the molecule is the same as in Figure 3.

tential (nucleophilic region) surround the N1–N2 bonds due to the high electronegativity of these atoms. In both maps, these regions have a kidney shape but exhibit a different expansion when we compare the results from experiment and theory. The minima of the negative electrostatic potential V_{min} are −0.174 (experiment) and −0.149 e Å^{-1} (theory), both close to N1.

The contraction of the region of negative electrostatic potential is due in part to the contribution of the positive charges carried by carbon and hydrogen atoms. This is particularly true for the negative pockets of electrostatic potential found in the vicinity of the nitrogen atoms N4 and N4′ from the theoretical calculations, which are not compensated by the positive contribution of H6 and H6′. These features are related to the less polarized electron densities of hydrogen atoms found in theoretical calculations, as men-

tioned above, but also to the more contracted lone pairs of nitrogen atoms. For the sake of comparison with related compounds, we have generated the electrostatic potential for isolated 2,2′-dimethyl-6,6′-diphenyl-4,4′-bipyrimidine[2] (**4**) and 2,2′-dimethyl-4,4′-bipyrimidine (**5**). For the latter, no experimental electron density is available and only DFT calculations were performed. The isosurfaces of the electrostatic potential are depicted in Figure 5. The experimental negative electrostatic potential surface corresponding to a cutoff of $-0.05\,e\,Å^{-1}$ extends from the phenyl ring to the bipyrimidine group (Figure 5, top) on both sides of **4**. From theoretical calculations, however, this negative region is limited in the vicinity of the inner (3-position in the pyrimidine ring) and outer (1-position) nitrogen atoms (Figure 5, center). When the phenyl rings are absent, the regions of negative electrostatic potential are found close to the inner and outer nitrogen atoms, as in **5** (Figure 5, bottom). The minimum values of the negative electrostatic potential are $V_{min\text{-}exptl} = 0.233\,e\,Å^{-1}$ and $V_{min\text{-}DFT} = -0.146\,e\,Å^{-1}$ (both close to N1) and $V_{min\text{-}DFT} = -0.159\,e\,Å^{-1}$ (close to N1 from theory) for **4** and **5**, respectively.

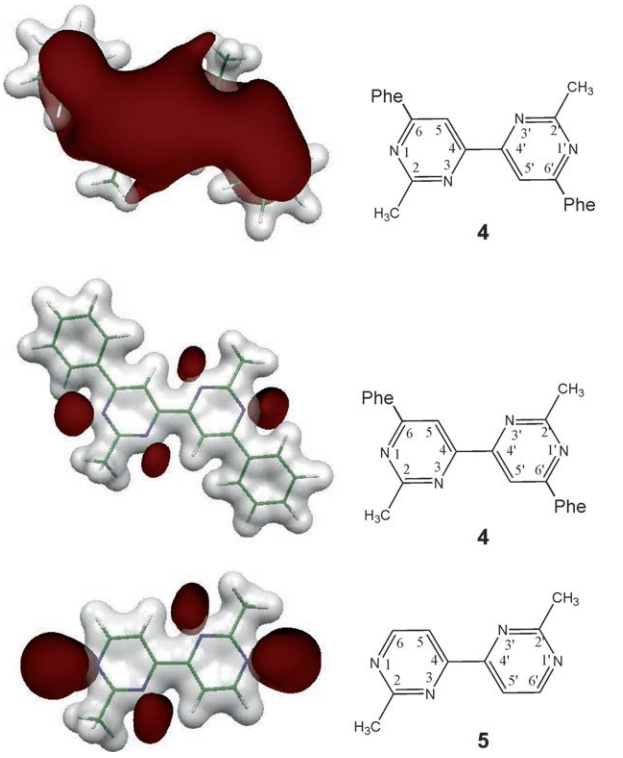

Figure 5. Electrostatic potential (left) of **4** (top: from experiment; middle: from theory) and **5** (bottom, from theory). Gray and dark red isosurfaces correspond to $+0.20$ and $-0.05\,e\,Å^{-1}$, respectively. Right: chemical structures of molecules.

Atomic charges of 3 and related molecules: In general, different types and definitions of atomic charges are used in the literature depending on the goals and methods. Charges are not physically observable and are model-dependent. This is the case for experimental charges derived from the so-called kappa refinement[15] or theoretical charges obtained, for instance, from a Mulliken population analysis.[16] The charges can also be fitted to the observed electrostatic potential (ChelpG charges) in order to reproduce this property.[17] The quantum theory of atoms in molecules (QTAIM) developed by Bader[18] is based on the partition of the electron density in atomic basins that allows integrated properties like atomic charges to be retrieved. Once the atomic basin is defined through the zero-flux surface of the gradient of the electron density, volume integration can be performed to obtain the charge. This method was applied to the title compound and to the related molecules **4** and **5**.

The program NEWPROP[19] can be used to retrieve the integrated charges from experimental charge densities. This calculation is based on a sophisticated analytical determination of interatomic surfaces. Recently, Henkelman et al. proposed a fast and robust numerical method based on steepest-ascent algorithm (BADERWIN program) to integrate the electron density on a fine grid.[20] In the steepest-ascent procedure, each grid point is assigned to the point where the electron density is maximum (nuclear attractor). As an example, Figure 6 displays the integration volumes of the nitrogen atoms in **3**. To compare the atomic charges obtained from both experiment and theory by a single method, we decided to use this new approach. As a benchmark, we also applied the NEWPROP procedure to the experimental electron density. The results are reported in Table 1. Compounds **4** and **5** have a planar bipyrimidine group and a center of inversion in the middle of the central C4–C4′ bond. Thus, Table 1 gives the atomic charges corresponding to half of each molecule. Both programs NEWPROP and BADERWIN give a difference in charges of symmetry-related atoms of around 0.001 e. Conversely, as mentioned above, the molecule of **3** is not planar and the integrations of the electron density over the entire molecule yield relatively higher discrepancies in the values of atomic charges for pseudo-symmetry-related atoms such as N4, N4′ and so on. The largest difference (0.2 e) is obtained for the pair C7, C7′ from NEWPROP calculations, even for a fine grid. The cor-

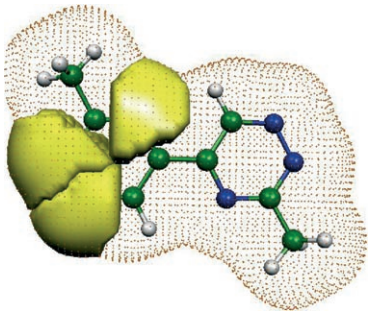

Figure 6. Integration volumes of the 1,2,4-triazine nitrogen atoms in **3**. The dotted surface corresponds to the $0.001\,e\,Å^{-3}$ isosurface of the total electron density. The orientation of the molecule is the same as in Figure 3.

Table 1. QTAIM charges (in *e* units) for **3**, **4**, and **5**. C and H atoms of methyl (meth) and phenyl (phe) groups are indicated in the atomic labels.

	3				**4**			**5**	
	EXP NEWPROP	EXP BADERWIN	DFT BADERWIN		EXP NEWPROP	EXP BADERWIN	DFT BADERWIN		DFT BADERWIN
N4	7.825	7.778	8.088	N1	7.929	7.958	8.077	N1	8.095
N4′	7.823	7.821	8.022	N3	8.071	8.153	8.149	N3	8.142
N1	7.377	7.397	7.455	C2	5.258	5.334	5.160	C2	5.156
N1′	7.363	7.534	7.484	C4	5.590	5.651	5.517	C4	5.510
N2	7.513	7.552	7.665	C5	6.135	6.152	5.988	C5	5.979
N2′	7.506	7.604	7.738	$C13_{meth}$	6.213	6.106	5.818	$C13_{meth}$	5.812
C5	5.606	5.573	5.534	C6	5.661	5.667	5.512	C6	5.454
C5′	5.591	5.741	5.661	$C7_{phe}$	5.903	5.784	5.934	H6	0.993
C6	5.569	5.486	5.382	$C8_{phe}$	6.130	6.190	6.033		
C6′	5.592	5.431	5.371	$C9_{phe}$	6.126	6.228	6.085		
C3	5.328	5.344	5.056	$C10_{phe}$	6.157	6.106	5.916		
C3′	5.294	5.307	5.017	$C11_{phe}$	6.135	6.119	5.997		
$C7_{meth}$	6.528	6.235	5.846	$C12_{phe}$	6.133	6.309	6.156		
$C7'_{meth}$	6.348	6.221	5.809	H5	0.834	0.810	0.954	H5	0.953
H6	0.905	0.902	1.001	$H131_{meth}$	0.830	0.906	1.070	$H131_{meth}$	1.069
H6′	0.898	0.896	1.002	$H132_{meth}$	0.831	0.798	0.972	$H132_{meth}$	0.972
$H71_{meth}$	0.897	0.952	1.033	$H133_{meth}$	0.845	0.844	0.988	$H133_{meth}$	0.982
$H72_{meth}$	0.750	0.740	0.955	$H8_{phe}$	0.831	0.831	0.939		
$H73_{meth}$	0.864	0.912	0.959	$H9_{phe}$	0.830	0.792	0.980		
$H71'_{meth}$	0.908	0.951	0.967	$H10_{phe}$	0.785	0.887	1.074		
$H72'_{meth}$	0.752	0.784	0.995	$H11_{phe}$	0.843	0.818	0.974		
$H73'_{meth}$	0.852	0.890	1.063	$H12_{phe}$	0.841	0.807	0.964		

relation between the experimental atomic charges of **3** and **4** obtained from programs NEWPROP[19] and BADERWIN[20] is excellent; the statistical factors are $R=0.999$, RMSD = 0.10 for **3** and $R=0.999$, RMSD = 0.07 for **4**. To our knowledge, it is the first time that the procedure implemented in the BADERWIN[20] program has been used for large molecules and the results are very encouraging. Excellent agreement factors ($R=0.999$ and RMSD = 0.02) were also obtained for the DFT theoretical charge sets of **4** and **5** molecules (Table 1). From consideration of electron withdrawal, the phenyl rings do not seem to modify the atomic charges in the heteroatomic groups like bipyrimidine. The respective theoretical electric charges carried by N1 (−1.077 e in **4** and −1.095 e in **5**) and N3 (−1.149 e in **4** and −1.142 e in **5**) are almost the same in **4** and **5**; the inner atom N3 is slightly more negative. Figure 7 compares the charges obtained from both experiment and theory for molecules **3** and **4** by using the BADERWIN program. A very good linear correlation appears with statistical factors *R* close to 1 and an RMSD of 0.2 e. The latter can be considered as a global standard deviation for the estimated charges. In **3**, the trend observed for **4** and **5** still remains: the inner nitrogen atom N4 carries the highest negative charge (−0.8 e from experiment and −1.0 e from theory). From both approaches (see Table 1), N2 (N2′) displays a slightly more negative charge than N1 (N1′), but the difference remains in the range of uncertainty (0.2 e).

Rotational energy barriers: The barriers for internal rotations about the central C–C bonds of structurally comparable molecules **3** and **5** in vacuo were calculated at the DFT level of theory. Total energies as functions of torsion angles were calculated by scanning these angles from 0° (*cis* form) to 360° at 10° intervals. The barriers for internal rotation were calculated as the difference between the total energy of the structure at each torsion angle, without any geometrical optimization, and that of the *cis* form of the molecule

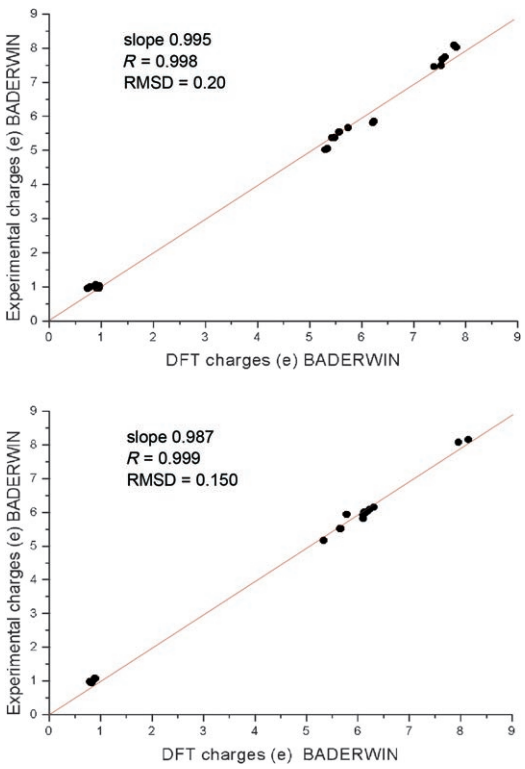

Figure 7. Experimental versus theoretical charges. Top: **3**. Bottom: **4**.

(torsion angle of 0°), taken as reference. Figure 8 shows this energy difference for **3** and **5**. As expected, the *trans* form (180°) is more stable than the *cis* form, by about 6.4 and

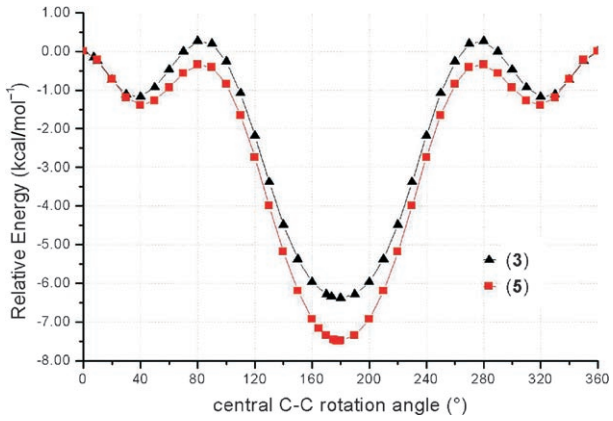

Figure 8. DFT energy barriers for internal rotation about central C–C bonds of **3** and **5**.

7.5 kcal mol^{-1} for **3** and **5**, respectively. This may be due to the H-bonding interactions between internal N4(N4′) and H6(H6′) for **3** and N3(N3′) and H5(H5′) for **5**, which stabilize the system. These nitrogen atoms carry the highest atomic charges (Table 1), probably because of this H-bonding interaction. For both molecules **3** and **5**, two local minima correspond to torsion angles of 40 and 320°. However, the local rotational barrier with respect to the maxima found at 80 and 280° is higher for **3** (1.43 kcal mol^{-1}) than for **5** (1.06 kcal mol^{-1}). This means that the energy demand of molecule **3** to reach its global minimum is higher by 0.4 kcal mol^{-1} with respect to **5**. Furthermore, the latter is more stable in its *trans* form by 1.1 kcal mol^{-1}.

Copper complexes of 4 and 5: The electrostatic properties derived from both theory and experiment show that the inner N3 and outer N1 nitrogen atoms of bipyrimidine-based molecules **4** and **5** have similar charges and topological features of the negative electrostatic potential. Accordingly, some years ago, we reported that both nitrogen atoms can participate in metal complexation[2] and we published crystallographic studies on several Cu^{I} bipyrimidine complexes.[2] In complexes, the ligands are in the *trans* form corresponding to the minimum of the rotational energy, as shown in Figure 8. It was also shown that different architectures can be obtained: for molecule **4**, isolated complex units, involving only the inner N3 nitrogen atoms, were found in the solid state, mainly due the steric hindrance of the phenyl groups; for **5**, however, in combination with a molecule of acetonitrile solvent, a polymer complex was obtained. In this case, both N1 and N3 participate in metal complexation. Figure 9 depicts the solid-state structures of the Cu^{I} complexes obtained from **4** and **5**.[2]

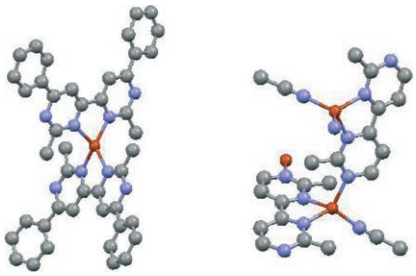

Figure 9. Structures of Cu^{I} complexes of **4** (left) and **5** (right). Hydrogen atoms are omitted for clarity. Copper atoms are in red and nitrogen atom in blue.

Copper complex of 3: Addition of a third nitrogen atom to the heterocycle to give a triazine should obviously increase the reactivity towards cations. The similar values of the atomic charges in **3** (Table 1) and the similar characteristics of the electrostatic potential (Figure 4) of the outer nitrogen atoms reinforce this hypothesis. This was experimentally demonstrated by the structure of the copper complex of **3** (**6**) displayed in Figure 10. In this structure, both *trans* and

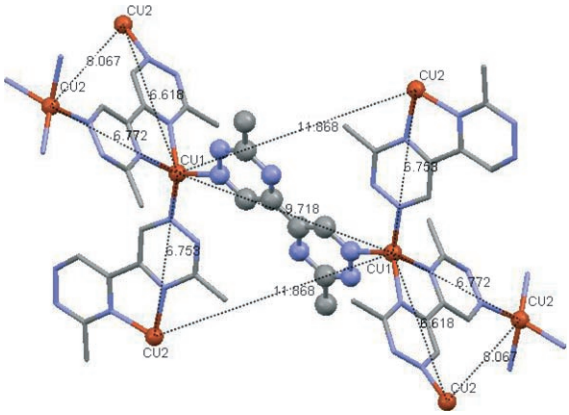

Figure 10. Crystal structure of the Cu^{I} complex of 3,3′-dimethyl-5,5′-bis-(1,2,4-triazine) **6**. Hydrogen atoms are omitted for clarity. Copper cations and the *trans* isomer of **3** are shown in ball-and-stick form. The distances between the copper cations are given in Å. Copper atoms are in red and nitrogen atoms in blue.

cis isomers, in the ratio 1:4, coexist in the solid state. Two copper cations, labeled Cu1 and Cu2 in Figure 10, were found in the asymmetric unit, both in tetrahedral coordination. Each copper cation is connected to four nitrogen atoms, two of which belong to the same bis-triazine molecule in *cis* form. For Cu1, the third bonded nitrogen atom is from another *cis* ligand, and the fourth from the *trans* isomer. However, no *trans* molecule is connected to Cu2. Only nitrogen atoms of type N4 (*cis* isomer, see Figure 1) and N1 (in both *cis* and *trans* ligands) are involved. Coexistence of both *cis* and *trans* isomers of ligand **3** agrees to some extent with the smaller energy barrier between these two forms reported above. The *trans* isomer of **3** bridges two copper cations, as shown in Figure 10 (Cu1–Cu1 9.718 Å),

exclusively through its outer N1, N1′ atoms. The nitrogen atoms corresponding to N2 of both isomers are never connected to any metal atom. Note that the absolute minimum of the electrostatic potential was found in the vicinity of N1 ($V_{min\text{-}exp} = -0.174$ e Å^{-1} and $V_{min\text{-}DFT} = -0.149$ e Å^{-1}), and this result agrees with the structure of the present copper complex. Each *cis* ligand of **3** is, in turn, bonded to three metal ions through N4, N4′ (Cu1), N1 (Cu2), and N1′ (Cu2′). The Cu–N bond lengths and angles are reported in Table 2. The

Table 2. Selected bond lengths [Å] and angles [°] in the copper complex of **3**.[a]

Bond lengths [Å]		Bond angles [°]	
Cu1–N1′A	1.993(8)	N1′A-Cu1-N1′C	110.9(3)
Cu1–N1C	2.018(9)	N1′A-Cu1-N4B	128.2(3)
Cu1–N4B	2.041(9)	N1′C-Cu1-N4B	111.7(4)
Cu1–N4′B	2.076(8)	N1′-Cu1-N4′B	119.6(3)
		N1C-Cu1-N4′B	99.4(3)
		N4B-Cu1-N4′B	80.5(3)
Cu2–N1′B#1	1.987(8)	N1′B#1-Cu2-N1B#2	97.2(3)
Cu2–N1B#2	1.991(9)	N1′B#1-Cu2-N4 A	124.0(3)
Cu2–N4A	1.991(9)	N1B#2-Cu2-N4 A	117.9(4)
Cu2–N4′A	2.055(8)	N1′B#1-Cu2-N4′A	112.2(3)
		N1B#2-Cu2-N4′A	127.2(3)
		N4A-Cu2-N4′A	80.8(3)

[a] A, B, C correspond to the three molecules found in the asymmetric unit. Symmetry operations: #1: $-1+x, y, z$; #2: $-1+x, {}^1/_2-y, {}^1/_2+z$

bond lengths are very similar to those reported for the complexes of **4** and **5**.[2]

Crystal architectures of the copper complexes of 3 and 5: Figure 11 depicts the crystal arrangements of the copper complexes of **3** and **5**. The bipyrimidine ligands **5** chelate the copper cations through two inner and one outer nitrogen atoms plus one from the acetonitrile solvent molecule. One outer nitrogen atom of the bipyrimidine molecule is never connected to any metal center. This gives rise to 1D zigzag chains in the solid state (Figure 11, top). These chains are isolated and parallel to the *b* axis in the crystal lattice. The distance between two adjacent copper cations is 6.12 Å. This is shorter than the Cu1–Cu2 distances of respectively 6.62, 6.75, and 6.77 Å (Figure 10) found in the copper complex of **3**, due to the *para* positions of the metal bonded nitrogen atoms (N1, N4). In the bottom part of Figure 11 (view down *a* axis) one particular view of the structure obtained for the copper complex of molecule **3** is shown. In this partial representation, each ligand **3** is linked to three metal atoms. This gives a cross-linked structure consisting of undulating chains (or branches) of alternating Cu1 and Cu2 atoms. The chains are interconnected via molecules **3** in *trans* form bonded exclusively to Cu1 cations (see Figure 10). In fact, both Cu1 and Cu2 atoms can be considered as the nodes of branches and this leads to a 3D polymer structure of the copper complex of **3**. Contrary to the structure of the copper complex of **5**, complexation of **3** gives rise to an novel multibranch network with open channels parallel to [101] (Figure 12), which resembles those of metal–organic frameworks

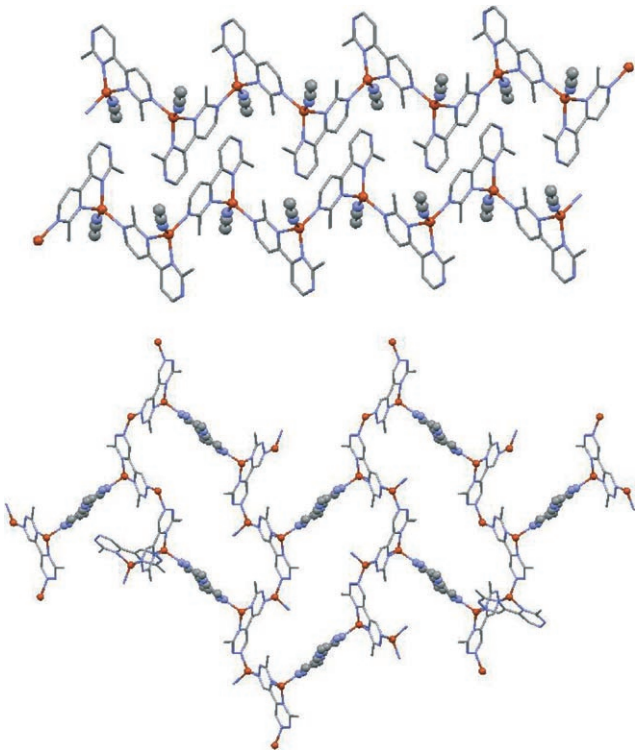

Figure 11. Crystal architectures of the copper complexes of **5** (top, copper and acetonitrile atoms are shown in ball-and-stick form) and **6** (bottom, copper cations and atoms of ligands **3** in *trans* form are shown in ball-and-stick form). Hydrogen atoms are omitted for clarity. Copper atoms are in red and nitrogen atoms in blue.

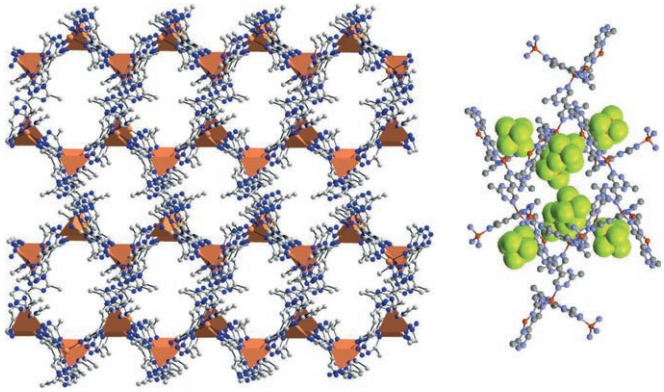

Figure 12. Left: View of channels in the structure of the copper complex of 3,3′-dimethyl-5,5′-bis(1,2,4-triazine) **6**. Copper tetrahedra are displayed. Right: the distribution of PF_6^- counterions (in space-filling form) in the empty spaces. Hydrogen atoms are omitted for clarity.

(MOFs) reviewed recently by Fletcher et al.[21] The PF_6^- counterions and solvent molecules occupy these channels. These anions are stabilized by multiple weak F···H hydrogen bonds with H atoms of the methyl groups of ligands **3**.

Conclusion

We have reported a new, efficient, and safer synthesis of 3,3′-dimethyl-5,5′-bis(1,2,4-triazine) that avoids the use of

potentially explosive reagents. Its crystal structure, established for the first time, shows that the molecule adopts an *s-trans* conformation in the solid state. Preliminary results on its complexation properties with metals were also reported, and spontaneous formation of a novel crystal network with Cu^{I} cations was demonstrated. In crystallization processes, kinetic factors are of significant importance. Nevertheless, we found a very good agreement between the complexation ability and the electronic features (from experiment or theory) of the isolated 3,3′-dimethyl-5,5′-bis(1,2,4-triazine) ligand without any kinetic or thermodynamic considerations. This shows that an intrinsic molecular property like the electrostatic potential is, to some extent, a good predictive index for metal chelation.

Experimental and Computational Section

General procedures: Solvents were purified by standard literature methods and reagents are used as received from Aldrich. Structures of all compounds were assigned by ^{1}H and ^{13}C NMR spectra recorded on a Bruker DRX 400 spectrometer. FTIR spectra were recorded on a Bruker Vector 22 spectrometer. UV/Vis spectra were recorded on a Safas Uvmc^{2}. Mass spectra were recorded on a Trio 1000 spectrometer in EI mode. Elemental analyses were determined on a Thermofinnigan Flash EA1112 analyzer.

Hydrazine–hydroquinone complex was synthesized by the literature method.[12]

Acetamidrazone (1): method A: A solution of acetamidine hydrochloride (8.0 g, 84.4 mmol) in MeOH was cooled in an ice bath (0–5 °C), hydrazine–hydroquinone complex (12.0 g, 84.4 mmol, 1 equiv) added, and the mixture stirred for 4 h affording an intense red solution. The solution was then concentrated in vacuo, and the residue crystallized from *n*-propanol at 0 °C overnight to give pure white crystals of acetamidrazone (5.61 g, 60 %).

method B: A mixture of hydrazine hydrate solution in water (5.0 g, 0.1 mol) and anhydrous $MgSO_4$ (3.0 g) was stirred under argon for 15 min. Then acetamidine hydrochloride (9.5 g, 0.1 mol) was added at 0–5 °C. The resulting reaction mixture was stirred for a further 4 h at the same temperature. The solution turned from pink to red. After filtration and evaporation of the solvent, pure acetamidrazone (11.0 g, 0.1 mol) was obtained quantitatively and used as is for the next step. IR (KBr): $\tilde{\nu}$ = 3356–3169 cm^{-1} (NH), 1697 cm^{-1} (C=NH); ESIMS: *m*/*z*: 74.4 $[M+H]^{+}$.

3-Methyl-1,2,4-triazine (2): method A: A mixture of acetamidrazone (5.0 g, 45.6 mmol) and $NaHCO_3$ (3.83 g, 45.6 mmol, 1 equiv) in diethyl ether (80 mL) was stirred at room temperature for 15 min. Glyoxal (7.85 mL, 68.4 mmol, 1.5 equiv) was added to the mixture. The solution became yellow and the mixture was stirred for a further 3 h. Then a saturated solution of NaCl (20 mL) was added, the aqueous phase was extracted with diethyl ether, and the organic phases were combined, dried over anhydrous $MgSO_4$, and filtered. The filtrate was concentrated under reduced pressure to afford a crude yellow mobile and volatile liquid (3.43 g, 79 %). ^{1}H NMR (400 MHz, $CDCl_3$, 25 °C): δ = 9.12 (s, 1H), 8.55 (s, 1H), 2.91 ppm (s, 3H). ESIMS: *m*/*z*: 96.4 $[M+H]^{+}$.

3,3′-Dimethyl-5,5′-bis(1,2,4-triazine) (3): method A: Solid KCN (0.5 g, 7.7 mmol) was added to a solution of **2** (0.20 g, 2.1 mmol) in water (15 mL) and stirred at 40 °C. The solution turned rapidly red then black and an intensely colored precipitate was immediate formed. The suspension was stirred for a further 1.5 h and then extracted with diethyl ether (250 mL). The ether phase was dried over anhydrous $MgSO_4$ and evaporated. The residue was purified by column chromatography on silica gel (Et_2O/hexane 7/3) to afford **3** (0.08 g, 0.4 mmol, 40 %) as an orange crystalline powder.

Method B: KOH (2.3 g, 41.04 mmol) and glyoxal (5.5 mL, 47.8 mmol) were added to a solution of acetamidrazone (5.0 g, 45.6 mmol) in water (30 mL). The mixture turned bright yellow after 15 min. K_2CO_3 (0.457 g, 4.56 mmol) was added. The reaction mixture was stirred for 3 h and then warmed to 40 °C. Then solid KCN (2.0 g, 30.8 mmol) was added, the color turned red and some precipitate appeared. The temperature was maintained for a further 1 h. After the stopper was opened, the reaction mixture turned black. After evaporation of water, the black residue was extracted by continuous stirring with diethyl ether (3.0 L). The organic phase was dried over anhydrous $MgSO_4$, filtered, and evaporated to afford **3** as an orange crude solid, which was crystallized from $CHCl_3$/hexane to afford pure bright yellow crystals (2.34 g, 12.4 mmol, 55 %). ^{1}H NMR (400 MHz, $CDCl_3$, 25 °C): δ = 10.08 (s, 2H; H-6), 2.97 ppm (s, CH_3); ^{13}C NMR (100 MHz, $CDCl_3$, 25 °C): δ = 167.8 (C-3), 151.1 (C-5), 144.7 (C-6), 24.2 ppm (CH_3); IR (KBr): $\tilde{\nu}$ = 3036 (CH arom.), 2926 (CH_3), 1537 (C=N), 1500 cm^{-1} (C=C); UV/Vis (MeOH): λ_{max} (ε) = 360 (9000), 290 nm (25 000 $mol^{-1}\,m^{3}\,cm^{-1}$); MS (70 eV): *m*/*z* (%): 188.2 (25) $[M]^{+}$, 160 (25) $[M-N_2]^{+}$, 91 (70) $[C_4HN_3]^{+}$; elemental analysis calcd (%) for $C_8H_8N_6$ (188): C 51.06, H 4.25, N 44.68; found: C 51.11, H 4.15, N 44.21.

Crystallization, data collection, and refinement of 3: Yellow crystals of **3** were grown from acetone. A crystal of good quality was chosen for high-resolution X-ray diffraction. The data were collected at 100.0(1) K on a Bruker-SMART CCD diffractometer using graphite-monochromated $Mo_{K\alpha}$ radiation. Cooling to 100 K was achieved with an N_2 gas stream (Oxford Cryosystems). The area detector surface was placed 4.02 cm from the crystal sample. The diffraction data were collected at different detector positions: 2θ = −60, −25, 0, +45, +75°. The data spots were recorded as ω scans ($\Delta\omega$ = 0.20°) to reconstruct accurate three-dimensional diffracted intensity profiles. According to the θ dependence of the diffracted intensities, the chosen exposure times were respectively 60, 30, 20, 45, and 90 s per frame for the detector positions given above. The maximum reciprocal resolution reached for this data set is $(\sin\theta/\lambda)_{max}$ = 1.10 $Å^{-1}$. Lorentzian polarization correction and the integration of the diffracted intensities were performed with the SAINT software package.[22] An empirical absorption correction was applied using SADABS.[22] Finally, SORTAV[23] was used for sorting and averaging equivalent and redundant data of high-resolution diffraction experiments. Table 3 lists the crystallographic data.

Structure and density refinements of 3: The crystal structure of **3** was solved and refined using WINGX software package.[24] Starting from these structural parameters, the conventional and electron density refinements were carried out using MOLLY program based on the Hansen–Coppens multipole model.[25] The frozen-core and valence spherical densities are calculated from the Hartree–Fock free-atom wave functions.[26] In this study, the ξ_l exponents (in $bohr^{-1}$) of the radial functions were chosen to be equal to 3.0, 3.8 and n_l = 2, 2, 3 up to octupole level (l = 3) for C and N atoms, respectively; ξ_l = 2.26 $bohr^{-1}$ and n_l = 1 (dipole level, l = 1) for the hydrogen atoms.[27] All the multipole parameters were obtained by least-squares fitting to the observed X-ray diffraction structure amplitudes *F*. Before the electron density refinement, the atomic positions and anisotropic thermal displacements for C and N were estimated from high-order data ($\sin\theta/\lambda \geq 0.8$ $Å^{-1}$). The C–H distances were constrained to the values observed by neutron diffraction ($C_{aromatic}$–H = 1.08 Å, C_{methyl}–H = 1.07 Å). All these structural and thermal parameters were relaxed in the last cycles of refinements. Figure 13 displays the map of residual electron density obtained after the multipole refinements. In this map, the absolute residues of the electron density do not exceed 0.20 e $Å^{-3}$, and this attests to good convergence of the refinements. The experimental errors in the electron density are $\langle\sigma^2(\Delta\rho)\rangle^{1/2}$ = 0.045 e $Å^{-3}$ and $\langle\sigma^2_{res}\rangle^{1/2}$ = 0.063 e $Å^{-3}$.[28,29]

Computational methods: The experimental atomic coordinates of **3** (this study) and **4**[2] were used for the theoretical calculations. For **5**, the phenyl groups in **4** were replaced by hydrogen atoms 1.08 Å from the attached carbon atom. Ab initio single-molecule calculations were performed with Gaussian 03[30] with DFT B3LYP/6-31G++(d,p) basis set.[31,32] For comparison with experimental electron deformation density maps $[\Delta\rho(r) = \rho_{molecule}(r) - \rho_{promolecule}(r)]$, the promolecule electron density

Table 3. Crystallographic data and refinement details of **3** and its copper complex **6**.

	3	**6**
empirical formula	$C_8H_8N_6$	$Cu_2(C_8H_8N_6)_{5/2}(PF_6)_2$-$(C_3H_6O)_x$[a]
formula weight	188.2	887.55
crystal system	monoclinic	monoclinic
space group	$P2_1/c$	$P2_1/c$
a [Å]	5.5158(1)	11.6531(7)
b [Å]	11.6940(2)	21.9875(13)
c [Å]	9.9613(1)	15.3104(9)
β [°]	100.765(1)	110.029(2)
V [Å^3]	860.09(2)	3685.6(4)
ρ_{calcd} [g cm^{-3}]	1.45	1.60
Z	4	4
T [K]	100(1)	100(1)
λ [Å]	0.71073	0.71073
μ [mm^{-1}]	0.100	1.34
crystal size [mm^3]	$0.20\times0.08\times0.06$	$0.20\times0.15\times0.08$
$F(000)$	392	1764
reflections collected	37598	24545
unique reflections	8962	9214
$(\sin\theta/\lambda)_{max}$ [Å^{-1}]	1.10	0.69
R_{int} [%]	3.6	10.6
Spherical refinement		
$R1[F^2>2\sigma(F^2)]$ [%]	5.12	11.93
$wR2(F^2)$ [%], S	15.7, 0.991	31.3, 1.03
reflections used $[F^2>2\sigma(F^2)]$	4909	4095
number of parameters	159	409
$(\delta/\sigma)_{max}$	0.000	0.001
$\Delta\rho_{max}$, $\Delta\rho_{min}$ [e Å^{-3}]	0.60, −0.47	2.32, −2.77
Multipole refinement		
reflections used $[F^2>3\sigma(F^2)]$	3316	
$R[F]$ [%]	2.74	
$R_w[F]$ [%]	2.27	
GOF	0.83	

[a] The number x of C_3H_6O solvent molecules could not be quantified.

(superimposition of spherically symmetrical densities of isolated atoms) was computed from the same basis set as for the calculation of the molecular density in order to minimize the errors due to the basis-set dependency.

Electrostatic potential: The electrostatic potential is the most important property that can reveal the interaction of a chemical system with other species. The highly positive electrostatic potential generated by the nuclei is compensated by the negative contribution of the surrounding electrons. Once the electron density is obtained, the calculation and plotting of the electrostatic potential is a convenient and instantaneous way to reveal the electrophilic and nucleophilic characters of a chemical system. Furthermore, in many cases, the interaction energy of molecular systems is dominated by the electrostatic part. This makes the electrostatic potential a predictive property of particular importance for the quantification of the chemical reactivity of molecules. In the present study, the electrostatic potential was generated on a 3D grid around the molecules by using the ELECTROS program[33] and the corresponding routine implemented in the Gaussian 03 package.[30] The MOLEKEL graphic software was used for visualizing the electrostatic potential.[34]

Crystallization and structure determination of copper complex of 3: Crystals of the complex $[(3,3'$-dimethyl-5,5′-bis(1,2,4-triazine$))_{5/2}Cu_2](PF_6)_2$ (**6**) were obtained after crystallization by slow evaporation of a solution in acetone. A suitable platelet-shaped, dark-brown crystal was glued to the top of a glass fiber for diffraction measurements at 100 K, collected on a Bruker-SMART CCD diffractometer with $Mo_{K\alpha}$ radiation. A conventional hemisphere data-collection procedure was used.[22] The crystal structure of the complex was solved and refined with the WINGX software package.[24] The hydrogen atoms were placed at idealized positions and refined by using the riding-atom method. Highly disordered acetone solvent molecules and PF_6^- counterions were observed in the crystal lattice channels. During the structure refinements, the number of acetone solvent molecules was difficult to estimate. Moreover, the peaks located in the void from the difference Fourier map could not be properly refined. Instead, a disordered solvent correction was applied using the SQUEEZE procedure[35] in the PLATON program.[36] The final residual factors were $wR2=0.313$ and $R1=0.119$. Crystallographic measurement and refinement details are given in Table 3. CCDC-628144 and CCDC-628145 contain the supplementary crystallographic data for the structures of **3** and **6** reported in this paper. These data can be obtained free of charge from the Cambridge Crystallographic Data Centre via www.ccdc.cam.ac.uk/data request/cif.

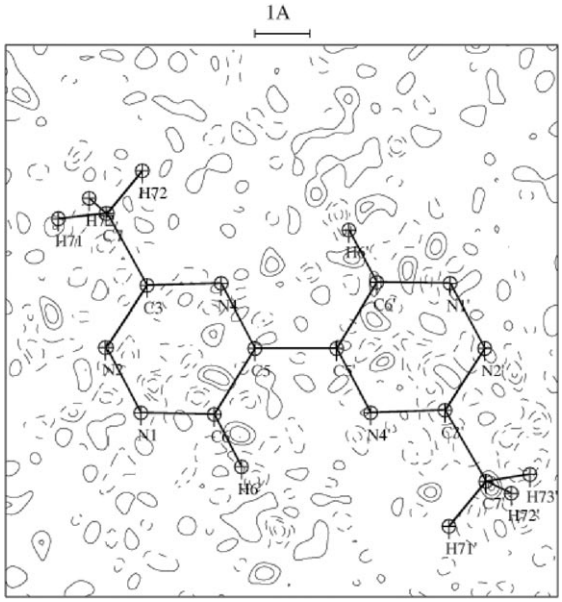

Figure 13. Map of residual electron density of **3** calculated with all data after multipole refinement. Contour intervals 0.05 e Å^{-3}; negative contours are dashed.

Acknowledgements

The financial support of the CNRS, Université Henri Poincaré-Nancy-1, Ecole Centrale Paris, and Université Paris XI is gratefully acknowledged.

[1] a) G. R. Newkome, A. K. Patri, E. Holder, U. S. Schubert, *Eur. J. Org. Chem.* **2004**, 235–254; b) C. Kaes, A. Katz, M. W. Hosseini, *Annu. Rev. Biophys. Biophys. Chem. Chem. Rev.* **2000**, *100*, 3553–3590; c) H. Hofmeier, U. S. Schubert, *Chem. Soc. Rev.* **2004**, *33*, 373–399; d) B. Machura, M. Jaworska, R. Kruszynski, *Polyhedron* **2005**, *24*, 2, 267–279; e) P. Govindaswamy, Y. A. Mozharivskyj, M. R. Kollipara, *J. Org. Chem.* **2004**, *69* 3265–3274; f) U. Arnold, O. Walter, M. Döring, *Inorg. Chim. Acta* **2006**, *359*, 1, 327–333; g) Y.-Q. Huang, B. Ding, H.-L. Gao, P. Cheng, D.-Z. Liao, S.-P. Yan, Z.-H. Jiang, *J. Mol. Struct.* **2005**, *743*, 1–3, 201–207.

[2] a) F. Bodar-Houillon, T. Humbert, A. Marsura, J.-B. Regnouf de Vains, O. Dusausoy, N. Bouhmaida, N. E. Ghermani, Y. Dusausoy, *Inorg. Chem.* **1995**, *34*, 5205–5209; b) N. E. Ghermani, N. Bouhmaida, C. Lecomte, A. L. Papet, A. Marsura, *J. Phys. Chem.* **1996**, *100*, 6287–6292.

[3] a) F. Bodar-Houillon, Y. Elissami, A. Marsura, N. E. Ghermani, E. Espinosa, N. Bouhmaida, A. Thalal, *Eur. J. Org. Chem.* **1999**, 1427–1440; b) J.-B. Regnouf de Vains, J.-M. Lehn, N. E. Ghermani, O. Dusausoy, Y. Dusausoy, A.-L. Papet, A. Marsura, P. Friant, J. L. Rivail, *New J. Chem.* **1994**, *18*, 701–708.

[4] a) S. Pellet-Rostaing, J.-B. Regnouf de Vains, R. Lamartine, P. Meallier, S. Guitonneau, B. Fenet, *Helv. Chim. Acta* **1997**, *80*, 1229–1243; b) K. Krause, R. A. Krause, S. Lamtruong, *J. Coord. Chem.* **1988**, *19*, 91–99.

[5] J. Mathieu, PhD thesis, University of Nancy (France), **2003**.

[6] a) J. Mathieu, B. Fraisse, D. Lacour, N. Ghermani, F. Montaigne, A. Marsura, *Eur. J. Inorg. Chem.* **2006**, 133–136; b) J. Mathieu, N. E. Ghermani, N. Bouhmaida, B. Fenet, A. Marsura, *Eur. J. Inorg. Chem.* **2004**, 5338–5346; c) F. Bodar-Houillon, A. Marsura, *Supramol. Chem.* **1998**, *9*, 191–198.

[7] K. Roussel, A. Cartier, A. Marsura, *Chem. Phys. Lett.* **2003**, *367*, 463–467.

[8] R. Jenssen, R. T. Pflaum, *Anal. Chim. Acta* **1965**, *32*, 235–244.

[9] a) D. K. Krass, T, -K. Chen, W. W. Paudler, *J. Heterocycl. Chem.* **1973**, *10*, 343–345; b) D. K. Krass, W. W. Paudler, *J. Heterocycl. Chem.* **1974**, *11*, 43–44; c) W. W. Paudler, R. E. Moser, N. M. Pollack, US 4105434, **1978**.

[10] a) H. Neunhoeffer, H. Hennig, H. W. Frühauf, M. Mutterer, *Tetrahedron Lett.* **1969**, *10*, 3147–3150; b) H. Neunhoeffer, F. Weischedel, *Liebigs Ann. Chem.* **1971**, *749*, 16–23.

[11] W. W. Paudler, T.-K. Chen, *J. Heterocycl. Chem.* **1970**, *7*, 767–771.

[12] F. Toda, S. Hyoda, K. Okada, K. Hirotsu, *J. Chem. Soc. Chem. Commun.* **1995**, 1531–1532.

[13] M. N. Burnett, C. K. Johnson, ORTEPIII, Oak Ridge Thermal Ellipsoid Plot Program for Crystal Structure Illustrations, Oak Ridge National Laboratory Report ORNL-6895, Oak Ridge, Tenessee, USA, **1996**.

[14] R. Destro, R. Soave, M. Barzaghi, L. Lo Presti, *Chem. Eur. J.* **2005**, *11*, 4621–4634.

[15] P. Coppens, T. N. Guru, P. Leung, E. D. Stevens, P. Becker, Y. W. Yang, *Acta Crystallogr. Sect. A* **1979**, *35*, 63–72.

[16] R. S. Mulliken, *J. Chem. Phys.* **1955**, *23*, 10, 1833–1840.

[17] C. M Breneman, K. B. Wiberg, *J. Comput. Chem.* **1990**, *11*, 361–373.

[18] R. F. W. Bader, *Atoms in Molecules: A Quantum Theory*, Oxford University Press, New York, **1990**.

[19] M. Souhassou, Atomic Properties from Experimental Electron Densities: Program Newprop-Int (LCM3B Internal Report, Université Henri Poincaré, Nancy 1, France), 19th European Crystallographic Meeting, Nancy, France, 25–31 August **2000**, Abstract No. S2-m2-p2, p. 195.

[20] G. Henkelman, A. Arnaldsson, H. Jonsson, *Comput. Mater. Sci.* **2006**, *36*, 354–360.

[21] A. J. Fletcher, K. M. Thomas, M. J. Rosseinsky, *J. Solid State Chem.* **2005**, *178*, 8, 2491–2510.

[22] Bruker SMART (Version 5.054), SAINT (Version 6.36A) and SADABS (Version 2.05), Bruker AXS Inc., Madison, Wisconsin, USA, **1998**.

[23] R. H. Blessing, *J. Appl. Crystallogr.* **1997**, *30*, 421–426.

[24] L. J. Farrugia, *J. Appl. Crystallogr.* **1999**, *32*, 837–838.

[25] N. K. Hansen, P. Coppens, *Acta Crystallogr. Sect. A* **1978**, *34*, 909–921.

[26] E. Clementi, D. L. Raimondi, *J. Chem. Phys.* **1963**, *41*, 2686–2689.

[27] E. Clementi, C. Roetti in *Atomic Data and Nuclear Data Tables, Vol. 44*, Academic, New York, **1974**, pp. 177–178.

[28] D. W. J. Cruickshank, *Acta Crystallogr.* **1949**, *2*, 65–82.

[29] B. Rees, *Acta Crystallogr. Sect. A* **1976**, *32*, 483–488.

[30] Gaussian 03, Revision B.04, M. J. Frisch, G. W. Trucks, H. B. Schlegel, G. E. Scuseria, M. A. Robb, J. R. Cheeseman, J. A. Montgomery, Jr., T. Vreven, K. N. Kudin, J. C. Burant, J. M. Millam, S. S. Iyengar, J. Tomasi, V. Barone, B. Mennucci, M. Cossi, G. Scalmani, N. Rega, G. A. Petersson, H. Nakatsuji, M. Hada, M. Ehara, K. Toyota, R. Fukuda, J. Hasegawa, M. Ishida, T. Nakajima, Y. Honda, O. Kitao, H. Nakai, M. Klene, X. Li, J. E. Knox, H. P. Hratchian, J. B. Cross, V. Bakken, C. Adamo, J. Jaramillo, R. Gomperts, R. E. Stratmann, O. Yazyev, A. J. Austin, R. Cammi, C. Pomelli, J. W. Ochterski, P. Y. Ayala, K. Morokuma, G. A. Voth, P. Salvador, J. J. Dannenberg, V. G. Zakrzewski, S. Dapprich, A. D. Daniels, M. C. Strain, O. Farkas, D. K. Malick, A. D. Rabuck, K. Raghavachari, J. B. Foresman, J. V. Ortiz, Q. Cui, A. G. Baboul, S. Clifford, J. Cioslowski, B. B. Stefanov, G. Liu, A. Liashenko, P. Piskorz, I. Komaromi, R. L. Martin, D. J. Fox, T. Keith, M. A. Al-Laham, C. Y. Peng, A. Nanayakkara, M. Challacombe, P. M. W. Gill, B. Johnson, W. Chen, M. W. Wong, C. Gonzalez, J. A. Pople, Gaussian, Inc., Wallingford, CT, **2004**.

[31] A. Becke, *J. Chem. Phys.* **1993**, *98*, 5648–5652.

[32] C. Lee, W. Yang, R. Parr, *Phys. Rev. B* **1988**, *37*, 785–789.

[33] N. E. Ghermani, N. Bouhmaida, C. Lecomte, ELECTROS, STATDENS, FIELD+: Computer program to calculate electrostatic properties from high resolution X-ray diffraction, Internal report UMR CNRS 7036, Université Henri Poincaré, Nancy 1, France and UMR CNRS 8612, Université Paris XI, France, **2001**.

[34] S. Portmann, H. P. Lüthi, MOLEKEL: An Interactive Molecular Graphics Tool, *Chimia* **2000**, *54*, 766–770.

[35] P. van der Sluis, A. L. Spek, *Acta Crystallogr. Sect. A* **1990**, *46*, 194–201.

[36] A. L. Spek, *J. Appl. Crystallogr.* **2003**, *36*, 7–13.

Received: November 24, 2006
Published online: February 7, 2007

